Boundary-Layer Meteorol (2010) 134:285–306
DOI 10.1007/s10546-009-9446-7

ARTICLE

Comparison of Observed, MM5 and WRF-NMM Model-Simulated, and HPAC-Assumed Boundary-Layer Meteorological Variables for 3 Days During the IHOP Field Experiment

Steven R. Hanna · Brian Reen · Elizabeth Hendrick · Lynne Santos · David Stauffer · Aijun Deng · Jeffrey McQueen · Marina Tsidulko · Zavisa Janjic · Dusan Jovic · R. Ian Sykes

Received: 24 January 2009 / Accepted: 2 November 2009 / Published online: 4 December 2009

Abstract The objective of the study is to evaluate operational mesoscale meteorological model atmospheric boundary-layer (ABL) outputs for use in the Hazard Prediction Assessment Capability (HPAC)/Second-Order Closure Integrated Puff (SCIPUFF) transport and dispersion model. HPAC uses the meteorological models' routine simulations of surface buoyancy flux, winds, and mixing depth to derive the profiles of ABL turbulence. The Fifth-Generation Pennsylvania State University/National Center for Atmospheric Research Mesoscale Model (MM5) and the Weather Research and Forecast-Nonhydrostatic Mesoscale Model (WRF-NMM) ABL outputs and the HPAC ABL parameterisations are compared with observations during the International H2O Project (IHOP). The meteorological models' configurations are not specially designed research versions for this study but rather are intended to be representative of what may be used operationally and thus have relatively coarse lowest vertical layer thicknesses of 59 and 36 m, respectively. The meteorological models' simulations of mixing depth are in good agreement (±20%) with observations on most afternoons. Wind speed errors of 1 or 2 m s^{-1} are found, typical of those found in other studies, with larger errors occurring when the simulated centre of a low-pressure system is misplaced in time or space. The hourly variation of turbulent kinetic energy (TKE) is well-simulated during the daytime, although there is a meteorological model underprediction bias of about 20–40%.

S. R. Hanna (✉)
Hanna Consultants, 7 Crescent Ave., Kennebunkport, ME 04046-7235, USA
e-mail: hannaconsult@roadrunner.com

B. Reen · D. Stauffer · A. Deng
Department of Meteorology, The Pennsylvania State University, University Park, PA, USA

E. Hendrick
Epsilon Associates, Maynard, MA, USA

L. Santos
Air Quality Associates, North Billerica, MA, USA

J. McQueen · M. Tsidulko · Z. Janjic · D. Jovic
NCEP, Camp Springs, MD, USA

R. I. Sykes
Sage Mgmt, Princeton, NJ, USA

At night, WRF-NMM shows fair agreement with observations, and MM5 sometimes produces a very small default TKE value because of the stable boundary-layer parameterisation that is used. The HPAC TKE parameterisation is usually a factor of 5–10 high at night, primarily due to the fact that the meteorological model wind-speed output is at a height of 30 m for MM5 and 18 m for WRF-NMM, which is often well above the stable mixing depth. It is concluded that, before meteorological model TKE fields can be confidently used by HPAC, it would help to improve vertical resolution near the surface, say to 10 m or less, and it would be good to improve the ABL parameterisations for shallow stable conditions.

Keywords Dispersion models · Evaluation of models · International H2O project (IHOP) · Mesoscale meteorological models · Surface fluxes of heat and momentum · Turbulent kinetic energy

1 Introduction

Many authors have recommended that improvements be made to methodologies where meteorological inputs are prescribed for air quality models (e.g., Pielke and Uliasz 1998; Pielke 1998; Seaman 2000). Most air quality model applications involve releases of chemicals at heights between the ground and about 1000 m, and the subsequent transport and dispersion take place in the atmospheric boundary layer (ABL), which has a typical depth during fair weather afternoons over land of 1–2 km. Most operational three-dimensional, time-dependent meteorological forecast models are focused more on predicting "weather" variables such as rainfall and maximum temperature, rather than variables that are of use to air quality models, such as mixing depths, wind profiles, and turbulence profiles. Nonetheless, many meteorological model configurations and methodologies have been developed with a focus on air quality scenarios (e.g., Seaman et al. 1995; Seaman 2000; Stauffer et al. 2000; Tanrikulu et al. 2000; Deng and Stauffer 2006). These applications generally use higher vertical resolution near the ground than that found in operational forecast applications. Note that the terms air quality model and transport and dispersion model are synonymous in the current paper.

Some researchers have evaluated meteorological model predictions of ABL variables with observations (e.g., Pielke 1998; Cox et al. 1998; Seaman 2000; Hanna and Yang 2001). It is found that stochastic variations in the atmosphere cause there to be a "minimum" uncertainty that cannot be simulated by the meteorological models, which results in a minimum root-mean-square error (RMSE). The minimum uncertainty for wind speed (U) is about 1 m s^{-1} in the ABL (Seaman 2000; Hanna and Yang 2001). The minimum uncertainty for wind direction (WD) at a height of about 10 m is largest at small U, and decreases approximately inversely proportional to U (the approximate relation is minimum RMSE (WD) $= 60^\circ/U$, where WD has units of degrees (°) and U has units of m s^{-1}). Hanna and Yang (2001) find that the minimum RMSE for the ABL height or mixing depth, z_i, is about 100 or 200 m for summer days with clear skies, when the mean z_i is about 1000 m. For clear nights with light winds, when z_i is very low, the minimum RMSE is of the same order as z_i itself (10 or 20 m), assuming that the meteorological model vertical resolution near the ground is 10 m.

The objective of the larger study in which the subject of the current paper is imbedded is to develop and evaluate improved operational meteorological inputs for the Second Order Closure Integrated Puff (SCIPUFF) transport and dispersion model, which was developed by Sykes et al. (2007) and is described and distributed as part of the Hazard Prediction Assessment Capability (HPAC) comprehensive modelling system by the Defense Threat Reduction Agency (2004). The current study uses version 4.04 of HPAC, which was originally

developed to use observations from nearby meteorological observing sites, and the model would internally calculate the needed meteorological profiles using standard ABL profile relations based on Monin-Obukhov (MO) similarity. However, HPAC has been undergoing transition towards the sole use of operational meteorological inputs provided in real time by forecast models (e.g., Stauffer et al. 2007). These forecasts of several meteorological models are accessible to HPAC in real time. The meteorological models being used for this purpose are intended to be representative of operational versions, with lowest vertical grid thicknesses of about 30–60 m, rather than special research versions with higher resolution. Currently HPAC uses the meteorological model outputs of surface buoyancy flux (B_o), ABL height z_i, and ABL profiles of wind speed (U), wind direction (WD) and temperature (T). At heights below the mid-point of the lowest meteorological model grid volume (about 18–30 m in the current study), the profiles of U, T and turbulent kinetic energy (TKE, e) are based on MO theory.

The question naturally arises whether the ABL inputs provided by the meteorological models agree with observations. Here, the meteorological model outputs and the HPAC simulations of some ABL variables are compared with observations from several near-surface sites in a flat rural area of dimensions about 600 km by 600 km. The 16 sites are in the USA Central Plains, where observations collected on 3 days (29 May and 6 and 7 June), from many days of extensive experiments in 2002 during the International H2O Project (IHOP, Weckwerth et al. 2004), are used for the comparisons of the Fifth-Generation Pennsylvania State University (PSU)/National Center for Atmospheric Research Mesoscale Model (MM5, described by Dudhia (1993) and Grell et al. (1995)) and the Weather Research and Forecast-Nonhydrostatic Mesoscale Model (WRF-NMM, described by Janjic 2003). We review below the IHOP field experiment, provide an overview of the models and their assumptions, and present the qualitative results of the comparisons.

This paper represents Phase I of the comparison study, and focuses on qualitative comparisons, such as vertical profiles and time series on which the observations and the meteorological model simulations are plotted. A few quantitative statements are included that describe approximate mean bias and scatter. The Phase II study, where statistical performance measures are being calculated, is still underway and results will be given at a later date.

2 The IHOP Field Experiment

2.1 IHOP Overview

IHOP took place during several weeks from 13 May to 25 June 2002. The field experiment and some highlights were described in a review article by Weckwerth et al. (2004), and some results are presented by LeMone et al. (2007a,b). Although the overall goal of IHOP is to further our knowledge of atmospheric water vapour and its effects on convection, the ABL component focused on case days without significant moist convection in order to better understand surface–ABL relationships under simpler, mostly, fair weather conditions. Possibly this knowledge could be applied to moist convective cases.

The IHOP dataset was chosen for use in the current comparisons because it has an extensive network of sonic anemometer observations of near-surface turbulence and turbulent fluxes, as well as high-resolution radiosondes released from several sites every 3 h. Figure 1 and Table 1 contain a map and a listing of names and locations of the 16 IHOP sites used in the current study. Three days were selected for analysis (29 May, 6 June, and 7 June) because of their use in other IHOP studies (Kang 2007; Kang et al. 2007; Reen 2007) and

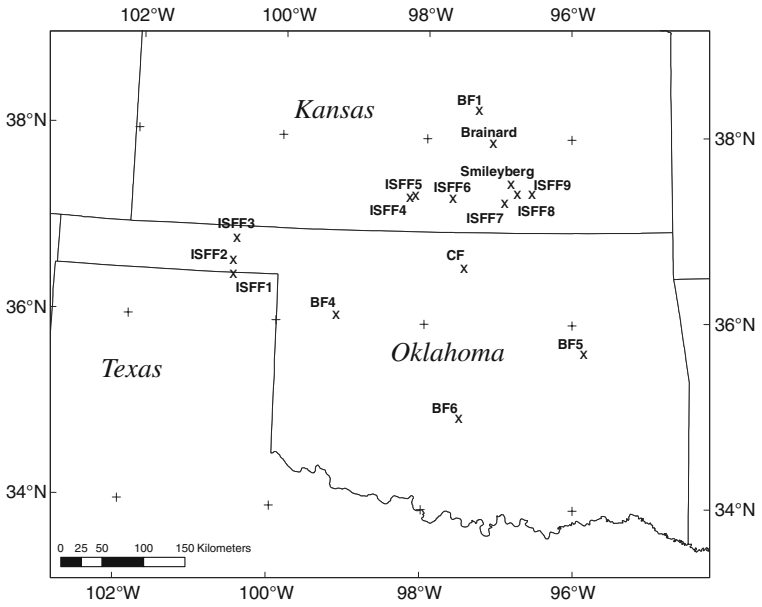

Fig. 1 IHOP observing sites in Oklahoma and Kansas used for comparisons. See Table 1 for details of the site locations

because they were typical of the period, with variable cloudiness, limited rain, and relatively complete data bases. On 29 May there was little daytime rain over most of the study area, and on 6 June and 7 June, there was almost no rain over the study region.

2.2 Descriptions of IHOP Observation Systems

Several datasets available in the IHOP data archive were investigated for use in these evaluations, as briefly described below.

2.2.1 Balloon-Borne Sounding System (SONDE)

The balloon-borne sounding system, also known as radiosonde or SONDE, provides observations of vertical profiles of winds, temperature, pressure and humidity. The SONDE data were obtained from http://www.arm.gov/instruments/instrument.php?id=sonde. We used radiosonde observations from the Central Facility in Lamont, Oklahoma (OK), USA, and from four other sites, at Hillsboro, Kansas (KS), USA; Vici, OK; Morris, OK; and Purcell, OK. Sonde profiles of temperature and relative humidity were plotted for every site and every 3 h for the 3 days and used to estimate the mixing depth z_i subjectively (by eye) for model evaluation.

2.2.2 Energy Balance Bowen Ratio (EBBR)

The Energy Balance Bowen Ratio (EBBR) system provides 30-min averaged estimates of vertical fluxes of sensible and latent heat. The estimates of "observed" sensible and latent heat fluxes were available at three IHOP EBBR locations [sites 1 (Lamont, OK CF),

Table 1 IHOP sites in Kansas and Oklahoma that are analyzed herein

Site number	Site name	Lat (°)	Lon (°)	MM5 Sfc rough z_o (m)	MM5 elev (m)	Radio sonde	Sonic anem	EBBR	ECOR
1	CF—Central Facility—Lamont, OK	+36.605	−97.485	0.15	311	X	X	X	LLNL
2	BF1—Hillsboro, KS	+38.305	−97.301	0.15	457	X		X	
3	BF4—Vici, OK	+36.071	−99.204	0.12	628	X			
4	BF5—Morris, OK	+35.688	−95.856	0.15	214	X		X	
5	BF6—Purcell, OK	+34.985	−97.522	0.15	348	X			
6	Smileyberg, KS	+37.521	−96.855	0.12	410		X		ANL
7	Brainard, KS	+37.960	−97.102	0.15	421		X		ANL
8	ISFF1	+36.473	−100.62	0.12	875		X		
9	ISFF2	+36.622	−100.63	0.14	846		X		
10	ISFF3	+36.861	−100.60	0.12	784		X		
11	ISFF4	+37.358	−98.245	0.12	500		X		
12	ISFF5	+37.378	−98.164	0.15	493		X		
13	ISFF6	+37.354	−97.653	0.15	406		X		
14	ISFF7	+37.313	−96.939	0.12	366		X		
15	ISFF8	+37.407	−96.766	0.12	427		X		
16	ISFF9	+37.410	−96.567	0.12	431		X		

Figure 1 shows the sites on a map of the area. *ISFF* Integrated Surface Flux Facility, *EBBR* Energy Balance Bowen Ratio, *ECOR* Eddy Correlation Flux Measurement System. The acronyms LLNL and ANL refer to Lawrence Livermore National Lab and Argonne National Lab, who provided the ECOR data indicated

2 (Hillsboro, KS BF1), and 4 (Morris, OK BF4) in Table 1] during the days studied. These data were obtained from http://www.arm.gov/instruments/instrument.php?id=ebbr.

2.2.3 Eddy Correlation Flux Measurement System (ECOR)

The ECOR system uses fast-response sonic anemometers to provide 30-min averaged measurements of surface turbulent fluxes of momentum, sensible heat and latent heat. These data are available from the website for much of the IHOP experiment period, though none were provided on the website for the 3 days of interest here. (We were able to obtain ECOR data for the Lamont, OK CF, from Ric Cederwall and Marc Fischer at Lawrence Berkeley National Lab.) The CF site had sonic measurements at two levels, 4 and 60 m, for May 29, and at one level, 60 m, for June 6 and June 7. The turbulent kinetic energy (e) was calculated from the observed ECOR turbulent energy components for comparison with the modelled TKE.

ECOR observations were also obtained from two other IHOP sites—Smileyberg, Kansas and Brainard, Kansas (sites 6 and 7 in Table 1). (These data were provided to us by David Cook of Argonne National Laboratory.) The sonic anemometers at these sites are at a height of 2.1 m. The Smileyberg site included other meteorological parameters measured by routine instruments (i.e., not sonic anemometers or special flux measuring instruments), such as temperature, relative humidity and wind speed and wind direction. These latter measurements were made at a height of 10 m.

2.2.4 Integrated Surface Flux Facility (ISFF)

The ISFF is designed to study exchanges between the atmosphere and the Earth's surface. There were nine ISFF measurement sites operating during the IHOP Experiment (sites 8–16 in Table 1), each having both propellor (at 10 m) and sonic anemometers (at heights ranging from 2.5 to 5 m). Time-averaged statistics of the variables were computed over 5- and 30-min periods. The turbulence variables are provided in the 5-min average datasets in the archive at http://www.eol.ucar.edu/rtf/projects/ihop_2002/isff/.

Thus the following IHOP ABL observations were analyzed: friction velocity u_*, TKE e, surface buoyancy flux B_o, mixing depth z_i, scalar wind speed U, wind direction WD, and temperature T.

3 Meteorological Models

The MM5 and WRF-NMM mesoscale meteorological models are used in the comparisons with the IHOP data. MM5 is a widely-used numerical model and WRF-NMM is the official forecast model used by the National Centers for Environmental Prediction (NCEP). These non-hydrostatic mesoscale models are often used as a primary input for HPAC. However, as pointed out earlier, these are intended to be representative of operational versions that are used every day so that meteorological model outputs are always available for use in HPAC. These models have coarser vertical resolution near the ground than special research versions of the same models designed to address this issue.

The MM5 simulations for two outer domains (36 and 12 km) start 12 h before the start of the case day (1200 UTC or 0600 LST) and are integrated for 36 h, while the 4-km domain that is the focus of this study starts 12 h later (0000 UTC or 1800 LST) and continues for 24 h (Fig. 2). The WRF-NMM simulations use a single 4-km domain (Fig. 2), which starts 12 h

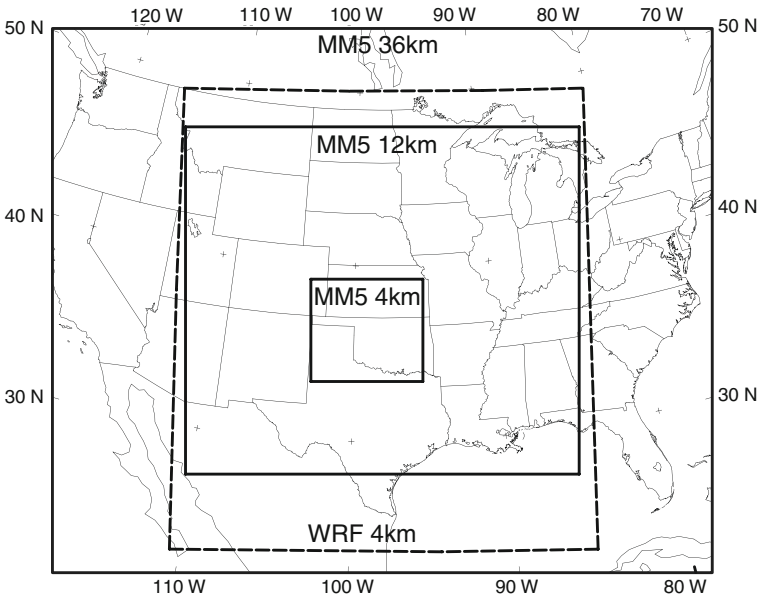

Fig. 2 MM5 and WRF-NMM modelling domains used for IHOP analysis. The MM5 nested grid domains (36, 12 and 4 km) are shown by the *solid lines* and the WRF-NMM 4-km domain is shown by the *dashed line*

prior to the 29 May case (28 May 1200 UTC) and at the 0000 UTC beginning time of the other 2 days. For all 3 days the WRF-NMM simulations integrate for 48 h. The starting times are either at 0000 or 1200 UTC since these are the world-wide standard radiosonde release times. Time series outputs were created at the 16 IHOP observation sites.

3.1 MM5

The MM5v3.6 is used but with the Noah land surface model (LSM, described by Chen and Dudhia 2001) updated to MM5v3.7.3. The domain analyzed here has a horizontal grid resolution of 4 km and 62 vertical sigma-pressure levels with the model top at 50 hPa. The MM5 uses Arakawa B-grid staggering (u and v wind components on the corners of the grid cell and mass in the centre). For the time series and profile analyses, the wind fields are interpolated to the mass field points and the closest mass field point to the observation site location is used. Due to vertical grid staggering, several variables are calculated at the layer interfaces (e.g., TKE, where the lowest full level above the surface is at 59 m above ground level, a.g.l.), while others are available in the middle of the layers (e.g., *T, u* and *v, WD*; the lowest half level is at approximately 30 m a.g.l.).

The Rapid Radiative Transfer Model (Mlawer et al. 1997) is used for longwave radiation and the Dudhia (1993) cloud-radiation scheme is used for shortwave radiation. Explicit microphysics including simple ice processes (no mixed phases, Dudhia 1993) is utilized. The Kain-Fritsch convective parameterisation (Kain and Fritsch 1990) is employed on the 36- and 12-km domains only.

The Gayno-Seaman (GS) TKE scheme (Stauffer et al. 1999, 2001; Shafran et al. 2000) is used and is coupled with the Noah LSM, since in the standard version of MM5 Noah is only coupled to other ABL schemes. The GS scheme is a level-2.5 closure (Yamada 1977)

meaning that the only second-order moment with a prognostic equation is TKE. The eddy diffusivity used to calculate vertical turbulent mixing is a function of TKE and length scales from Ballard et al. (1991) that are dependent on the Blackadar length scale (Blackadar 1962), TKE, buoyancy, and shear. The thermodynamic variable used for mixing is liquid water potential temperature (ice-water liquid potential temperature if ice processes are present). Four stability regimes are used in GS that are calculated based on z_i, L, and bulk Richardson number (Ri_b, calculated using the temperature difference between the ground and the lowest model half layer (here ≈30 m) and wind speed at ≈30 m). The stable regime is defined as ($Ri_b \geq 0.2$).

In the GS TKE scheme, the mixing depth z_i is estimated as the first layer where TKE falls below the smaller of, (a) 0.1 $m^2\ s^{-2}$ and (b) half of the maximum TKE in the column. The 0.1 $m^2\ s^{-2}$ criterion works well in situations with strong TKE but was found not to work well in special cases where a mixed layer exists with weak TKE (e.g., stratocumulus layers over the ocean, Stauffer et al. 2001). The "half of the maximum TKE in the column" criterion works well in the special cases and has been found to work reasonably well in some cases over land with stable stratification (e.g., where there is only weak shear-driven turbulence). There are a few exceptions to this methodology:

1. If maximum TKE or TKE at the lowest model level is less than 0.04 $m^2\ s^{-2}$, then z_i is diagnosed as the first model full layer above the ground (here ≈59 m).
2. If in the stable regime (bulk Richardson number $[Ri_b] > 0.2$) then z_i is set to zero. This is not to say that z_i is non-zero, but, (a) with typical MM5 vertical resolution we cannot accurately diagnose z_i, (b) TKE predictions in GS for stable conditions have not been evaluated sufficiently, and (c) it is not clear that model TKE is the best model predictor of z_i in stable conditions.
3. If z_i is diagnosed greater than 5000 m then it is set to 5000 m. This limits problems when moist convection may result in very high mixing depth diagnoses and limits numerical issues that may occur if z_i outside moist convection reaches above this height.

The GS scheme was originally formulated such that during stable conditions a simpler first-order non-TKE ABL methodology known as the Blackadar ABL (Zhang and Anthes 1982) was used. Therefore no TKE was calculated during stable conditions. However, TKE is now calculated in GS for all regimes. During stable conditions TKE is often smaller than the assumed background (minimum) value of 0.001 $m^2\ s^{-2}$, and so the TKE field defaults to 0.001 $m^2\ s^{-2}$. Since the vertical resolutions typical for mesoscale models are too coarse to accurately resolve the small z_i (of a few tens of m. or less) for stable conditions, limited attention has generally been paid in the GS scheme (and other ABL schemes) to the performance of the TKE predictions during stable conditions. Thus, there is limited confidence in the TKE predictions during stable conditions (unless model vertical resolution is greatly enhanced; Stauffer et al. 2001). Therefore with standard model vertical resolutions, we recommend not using TKE during stable conditions, especially to determine a reliable z_i. It probably makes more sense to consider either a L or roughness-length based approach, or as a default, make z_i equal to the lowest model grid half-depth (here ≈30 m). The MM5-GS developers are considering such an approach for implementation into the GS scheme. For all other regimes (i.e., other than the stable regime) TKE should be used.

The initial conditions and lateral boundary conditions for the coarse domains were defined using the Eta Data Assimilation System (EDAS) analyses enhanced using surface and rawinsonde data by a modified successive scan objective analysis method (Benjamin and Seaman 1985). The EDAS analyses enhanced by observations were also used on the coarse domains

for analysis nudging (Stauffer and Seaman 1994) above the ABL. An offline Noah simulation forced by observations provided initial conditions for Noah (Chen et al. 2007).

3.2 WRF-NMM

The WRF-NMM (Nonhydrostatic Mesoscale model) V2.1.16 (12/19/06 version, Janjic 2003) was used, employing the Central USA configuration with 4-km horizontal resolution [see Fig. 2; expanded contiguous USA, 1.6 times smaller than the full North American Mesoscale (NAM) domain] and 60 sigma-pressure hybrid vertical levels with the model top at 50 hPa. The model is run on a rotated latitude-longitude grid with Arakawa E-grid staggering (same as B staggering but rotated 45°). Due to vertical grid staggering, some variables are calculated at the layer interfaces (e.g., e, where the lowest full level above the surface is at approximately 36 m a.g.l.), while others are available in the middle of the layers (e.g., T, U, WD; the lowest half level is at approximately 18 m a.g.l.).

The model physics and dynamics are the same as those in the operational NAM with Ferrier cloud microphysics, Betts-Miller-Janjic convective parameterisation, Mellor-Yamada Janjic (MYJ) TKE-based planetary boundary-layer parameterisation, the Noah land surface model and the Geophysics Fluid Dynamics Lab (GFDL) Lacis-Hansen radiation.

The NMM MYJ ABL scheme (Janjic 1996a,b, 2001) has been used in the NCEP operational WRF since 2006 and in the previous NCEP operational mesoscale model, Eta. The MYJ is a level-2.5 scheme (e is the only second-order moment with a prognostic equation) presented in detail in Janjic (2001). The eddy diffusivity used to calculate vertical turbulent mixing is a function of TKE, a master length scale, and a term dependent on TKE, buoyancy, and shear. The thermodynamic variable used for mixing is liquid water potential temperature. The master length scale is diagnosed in the ABL in the unstable range with the requirement that the e production be non-singular in the case of growing turbulence, and in the stable range with the requirement that the ratio of the vertical velocity deviation variance and TKE cannot be smaller than that corresponding to the regime of vanishing turbulence. Above the ABL it is computed as a fraction of the vertical grid size. The first guess of the master length scale is then reduced if necessary in order to remain below an upper limit proportional to $\sqrt{e}$ and a function of buoyancy and shear of the mean flow. The empirical constants needed in this TKE scheme are derived from observations.

Note that z_i is diagnosed where e reaches a critical minimum value of 0.101 $m^2\ s^{-2}$, which is just above the assumed background TKE value of 0.100 $m^2\ s^{-2}$. For situations when calculated TKE is less than or equal to the minimum value (and thus the minimum TKE is invoked) at all levels, z_i is set to the first model layer depth. Recall that MM5 assumed a background TKE that is 100 times smaller (i.e., 0.001 $m^2\ s^{-2}$).

Atmospheric states were initialized with WRF standard initialization (SI)/REAL from EDAS/Eta forecasts. Lateral boundary conditions come from the NCEP Global Forecast System (GFS) with initial conditions from the NAM 3-D variational Data Assimilation System (NDAS) as configured during IHOP. The NDAS assimilates surface, radiosondes, profiler winds, Aircraft (Aircraft Communication Addressing and Reporting System; ACARS) meteorological data as well as satellite direct radiances from Geostationary Operational Environmental Satellite (GOES), Advanced Very High Resolution Radiometer (AVHRR) and Solar Backscatter UltraViolet radiometer (SBUV) satellites.

The land surface was initialized with the Gayno-Gridgen utility from EDAS land states at the initial time (but WRF land states were allowed to evolve with time). The EDAS soil moisture was scaled to current new operational 24 class soil types in WRF-NMM. The Noah

land surface model is continuously cycled with variables including observed precipitation from the NWS River Forecast Center (RFC) gridded estimates.

4 HPAC/SCIPUFF Meteorological Parameterisations Used in Comparisons

Given the set of MM5 outputs for the IHOP periods, it is necessary to convert them to the Multiscale Environmental Dispersion Over Complex terrain (MEDOC) format for direct input to the HPAC transport and dispersion model, SCIPUFF (Sykes et al. 2007). The conversion is necessary so that the MM5 outputs are input to HPAC at its specified horizontal grid points and vertical levels defined to be similar to those of the MM5. Future improvements to the conversion interface software include using native meteorological grids in SCIPUFF. In the current study, only the MM5 fields were converted to MEDOC format, since the WRF conversion was not yet available. The MEDOC file includes ABL variables such as z_i, B_o, and vertical profiles of U, WD, and T. HPAC uses the MEDOC files of B_o at each grid location, and U at the top of the lowest grid volume, combined with standard ABL profile formulae, to calculate u_*, L, and vertical profiles of turbulent wind components (σ_u, σ_v, and σ_w) and Lagrangian time scale components.

Because HPAC directly uses MM5 U and T at heights above the lowest level, we do not compare HPAC parameterisations with meteorological model simulations of these variables. The same can be said of z_i and SBF. However, for HPAC parameterised variables such as u_*, TKE, and U and T profiles within the lowest model grid volume, the HPAC variables are included in the comparisons.

5 Methods Used for Comparisons

The MM5 and WRF-NMM model simulations, the HPAC/SCIPUFF parameterisations (of u_* and e), and the observed meteorological variables are compared. As stated earlier, the current paper focuses on the Phase I qualitative comparisons and a few simple quantitative conclusions, while a future study will present the detailed quantitative model performance comparisons.

It is stressed that these are configurations intended to be representative of the operational meteorological models that are being used in these comparisons. The higher resolution versions of the models were not used because they are currently not part of the set of meteorological models used by HPAC. Most of the IHOP nighttime ABL data that are analyzed here are quite stable, meaning that better vertical resolution near the ground would probably improve the comparisons with observations.

We note that there is somewhat of a mismatch in the effective averaging times and distances in this comparison. The meteorological model (MM5 and WRF-NMM) simulations represent an average over a three-dimensional grid volume, with thickness of approximately 36 m (WRF-NMM) to 59 m (MM5) next to the ground and a horizontal grid cell size of 4 km. The model simulations at small timesteps are combined to form 5- and 30-min averages. In contrast, the sonic anemometer observations, averaged over the same 30-min period, represent a single point within the much larger model grid volume. Clearly the point observation will have more variability than the volume average.

The turbulence comparisons are of some concern, because the meteorological models simulate only the total TKE and do not provide its three components. But any dispersion model (e.g., HPAC) needs the three components to calculate the rate of dispersion in the

three directions. In the current exercise, we can compare only the observed, meteorological model simulated, and HPAC parameterised total TKE.

Another concern with the TKE comparison is that at 4-km horizontal grid spacing the meteorological model simulates the sub-grid TKE, and assumes that the model resolves the flow (and hence the "turbulence") at scales larger than the grid size (although based on kinetic energy spectra, the effective resolution of a mesoscale model is approximately seven grid cells; Skamarock 2004). However, the sonic anemometer TKE accounts for all observed fluctuations during the 30-min time period, including the fluctuations associated with scales larger than the model resolution.

With these caveats, we have proceeded with the following qualitative comparisons

- Mixing depths z_i from MM5 and WRF-NMM are compared with those estimated by eye from the radiosonde T and RH profiles, taken every 3 h.
- Profiles are available from MM5 and WRF-NMM in the ABL at height increments of about 50–100 m. The profiles of simulated variables U, WD, and T are compared with the observed radiosonde profiles of these variables. Profiles of simulated e are compared with sonic anemometer observations at two levels (4 and 60 m) at the Lamont, OK, CF site.
- Time series of meteorological model simulated u_* and TKE are compared with HPAC parameterisations of these variables. HPAC uses meteorological model simulations of z_i, B_o, and an assumed z_o to make these calculations. The observations of u_* and e were made at $z = 2$ to 4 m at all sites. In addition, at the Lamont, OK, Central Facility site, an observation was also available at $z = 60$ m.
- Time series of MM5 and WRF outputs of several other variables (i.e., B_o, U, WD and T) are compared with the near-surface observations at all 16 sites.

MM5 and WRF-NMM model outputs are provided in a time series format, with averages in 5- and 30-min blocks. The 5-min averages of U, WD, and T are used in radiosonde profile comparisons. The 5-min averages are also used in the time series comparisons with the ISFF observations. The 30-min averages are used in the vertical profile comparisons of TKE at Lamont and in the time series comparisons at sites 1, 6, and 7 (Lamont, Smileyberg and Brainard).

When a U time series is plotted for comparison with the observations at the 60-m level of the CF tower, the MM5 and WRF-NMM wind speeds are adjusted upwards from the model level immediately below the observation height using a logarithmic profile relation, implying that neutral conditions are assumed. Other variables were not extrapolated or interpolated in the vertical and, in this case, the height of the variable is shown on the plot.

There have been over 1000 comparison plots generated in this study, including the vertical profiles and time series of the many variables at 16 sites for 3 days. We have chosen a small fraction of these to include and discuss below. The plots shown are just examples used to illustrate potential weaknesses in the application of mesoscale meteorological model data into a transport and dispersion model and were not selected to represent "best" or "worst" performance.

6 Comparisons of Vertical Profiles

Of the 720 vertical profile plots that were generated (3 days with eight profiles per day at five locations and six variables), four sample profile figures are presented and discussed. Mixing depths were estimated subjectively by eye from each observed radiosonde profile of T and

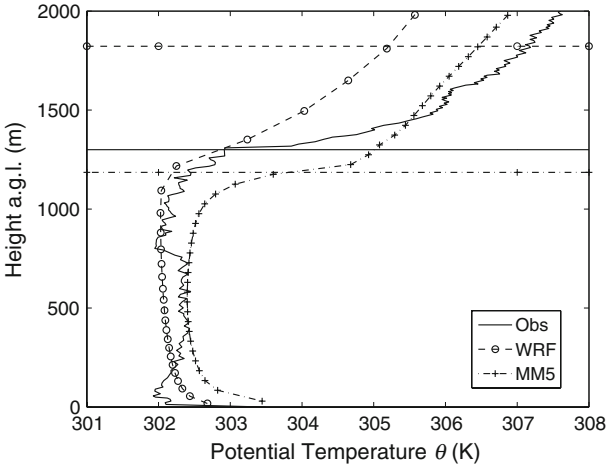

Fig. 3 Example of daytime θ profile comparisons, to 2000 m, for the Lamont Central Facility at 1430 LST on 29 May. The WRF and MM5 profiles are 5-min averages

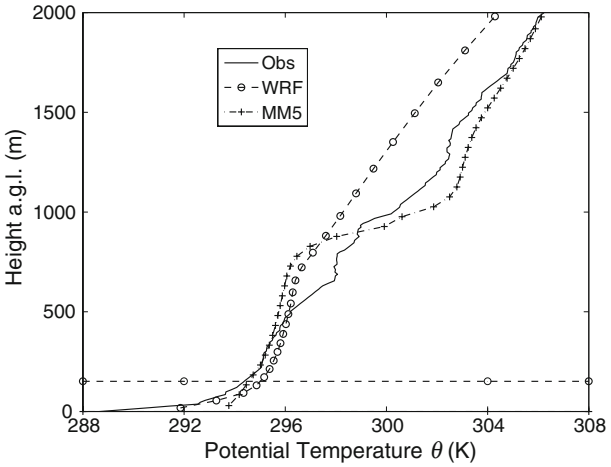

Fig. 4 Example of nighttime θ profile comparisons, to 2000 m, for the Lamont Central Facility at 0241 LST on 29 May. The WRF and MM5 profiles are 5-min averages. The MM5 diagnosed a mixing depth z_i of zero. Mixing depth z_i could not be estimated from the radiosonde observations

RH. As anyone who has analyzed large numbers of radiosondes profiles soon discovers, the "textbook" shapes for *T* and *RH* profiles do not always occur in reality.

Figure 3 compares the observed and simulated potential temperature, θ, profiles and mixing depths, z_i, for the Lamont, OK, Central Facility site for 1430 LST on 29 May 2002 (5-min average shown for WRF and MM5). This is a "textbook" afternoon profile with a clear capping inversion and observed mixing depth of 1310 m. It is seen that the MM5 θ profile is similar to the observed profile, although the simulated capping inversion is about 120 m lower than that observed, close to the base of the MM5-simulated capping inversion. The WRF-NMM's θ profile is also close to the observed profile. But the WRF-NMM z_i estimate is about 1800 m, which is about 600 m higher than its own capping inversion base,

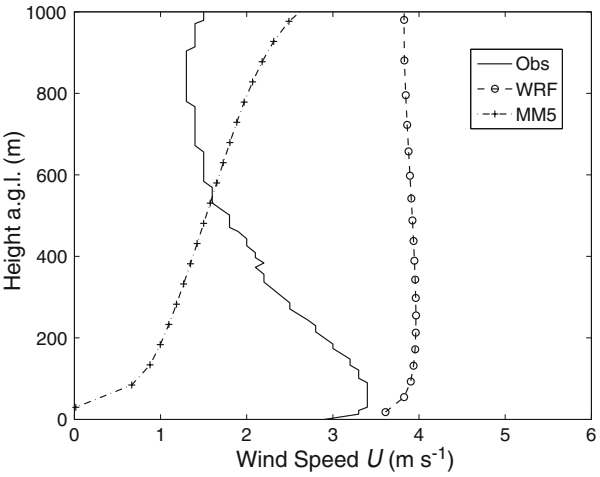

Fig. 5 Example of daytime U profile comparisons for the Lamont Central Facility at 1430 LST on 29 May. The WRF and MM5 profiles are 5-min averages

and is about 500 m larger than the observed. This trend with WRF-NMM is seen in most of the radiosonde profiles.

Figure 4 is the same type of plot as Fig. 3, except for a nighttime stable period (0241 LST) at Lamont on 29 May. The observed θ profile has a 4°C surface inversion in the lowest 40 m, with a steady and more gradual θ gradient (about 1°C per 100 m), above that. WRF-NMM simulates the surface inversion. MM5 has a near-adiabatic layer near the surface in this profile due to cloud, but an inversion does form in MM5 profiles 2 or 3 h after this figure. WRF-NMM simulates the observed deep slightly stable layer above the surface inversion. MM5 has a 6°C capping inversion between 800 and 1100 m. The observed z_i is indeterminate because of the strong ground-based inversion with a deep slightly stable layer above that. MM5 does not estimate z_i because of the ground-based inversion. The simulated z_i for WRF-NMM is 150 m, based on its TKE criterion, and appears to be an overestimate.

Observed and simulated profiles of wind speed, U, were also compared and found to show much variability. The observed winds themselves were variable in space and time across the IHOP domain, because fronts, clouds and light rain occurred occasionally within the domain. The meteorological model simulated winds were also variable, and disagreements with observations at specific times and locations could be seen even though the meteorological model may have successfully simulated the formation of a cloud area or a front. This is because the meteorological model timing might be a few hours off in the frontal passage or the model might displace the centre of a small wave by a few grid points.

As an example of the many U profile plots, Fig. 5 shows the profile for Lamont, OK, at 1430 LST on 29 May. This is the same location and time used for the temperature profile comparison in Fig. 3. Note that the observed winds are about 3.0 to 3.5 $\mathrm{m\,s^{-1}}$ in the 100 m layer near the surface and gradually decrease to about 1.2 $\mathrm{m\,s^{-1}}$ at a height of 800 m. The WRF-NMM simulated winds are nearly uniform with height, but at about 4 $\mathrm{m\,s^{-1}}$ (i.e., 1–2 $\mathrm{m\,s^{-1}}$ greater than the observed). The MM5 simulated winds, on the other hand, are light (less than 1.2 $\mathrm{m\,s^{-1}}$) in the lowest 200 m and slowly increase to 2 $\mathrm{m\,s^{-1}}$ at $z = 800$ m. If the HPAC model were to simulate a pollutant release near the ground, the effective cloud speed would be much different depending on which wind speeds were used—the observed, the MM5, or the WRF-NMM.

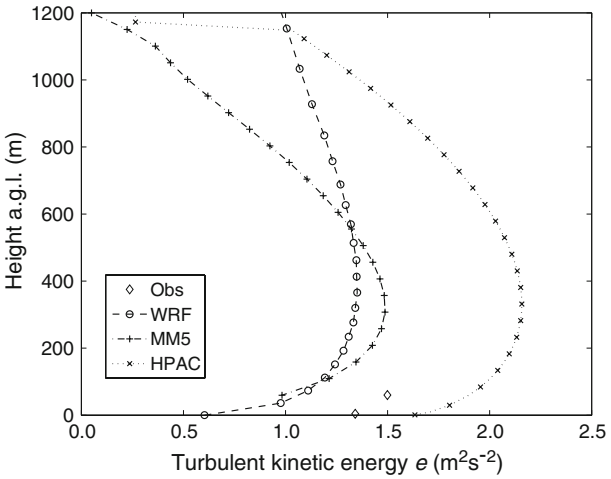

Fig. 6 Example of daytime e profile comparisons for the Lamont Central Facility at 1430 LST on 29 May. The WRF and MM5 profiles are 5-min averages

The e profile comparisons are of special interest because of the desire to incorporate meteorological model TKE fields as inputs to HPAC. As stated earlier, the Lamont, OK, site was the only one with an observed profile of e, at heights of 4 and 60 m. Figure 6 shows the observed, the HPAC-parameterised, and the MM5 and WRF-NMM-simulated TKE profiles for the same time (the afternoon of 29 May) and location as Figs. 3 and 5. The plotted meteorological model TKE is based on a 5-min average. Observed TKE is 1.3 and 1.5 $m^2\ s^{-2}$ at heights of 4 and 60 m, respectively. The MM5 and the WRF-NMM-simulated TKE values are about 30% smaller than the observations at the 60-m observation height. MM5 does not simulate TKE below 59 m, while WRF-NMM uses u_* to create a diagnostic value of TKE at the surface that is about a factor of two less than observed. The HPAC-parameterised TKE is about 20% larger than the observations. Recall that HPAC calculates e on its own, based on its estimate of u_* using MM5-simulated U, z_i, and SBF, and its assumed z_o. The HPAC TKE is about 0.7 $m^2\ s^{-2}$ larger than the MM5 value at heights above 100 m. This is about 50% larger than the MM5 values at heights of 200–700 m, but is a factor of three or more larger at heights above 1000 m and approaching the mixing depth.

7 Comparisons of Diurnal Time Series

A total of 216 diurnal time series plots (3 days for 12 sites for six variables) have been analyzed. A few examples of plots are described below. As mentioned earlier, these do not intentionally show best or worst cases.

7.1 Comparisons of T, WD, U, u_*, e, and B_o Time Series for the Lamont Central Facility Site for the 3 Days

This section discusses the time series for one of the 12 sites—the Lamont, OK Central Facility. Discussions refer to the 60-m observing level for three days and for six variables (T, WD, U, u_*, e, and B_o). However, only two of the 18 available plots are shown. Figures 7

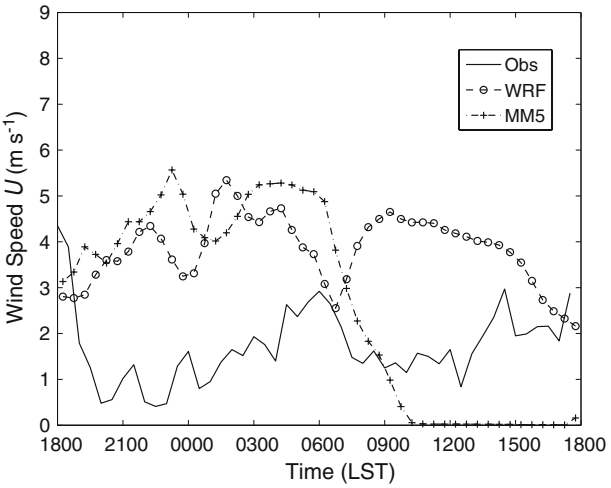

Fig. 7 Observed ($z = 60$ m) and simulated (WRF 55 m adjusted as described in text to 60 m, MM5 30 m adjusted to 60 m, HPAC 60 m) U at Lamont Central Facility for 1800 LST May 28 through 1800 LST May 29. The WRF and MM5 time series points are 30-min averages

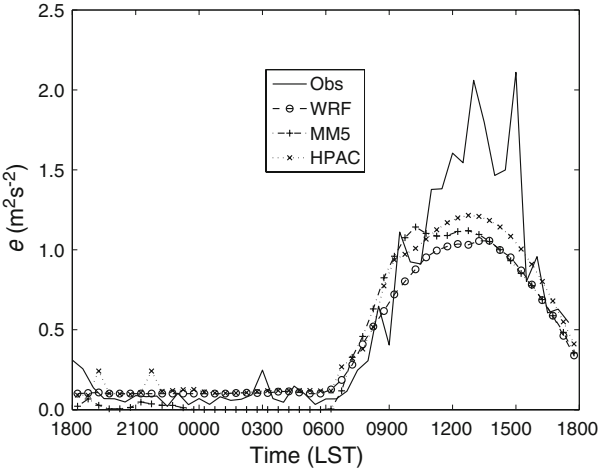

Fig. 8 Observed ($z = 60$ m) and simulated (WRF 36 m, MM5 59 m, HPAC 60 m) TKE at Lamont Central Facility for 1800 LST 28 May through 1800 LST. The WRF and MM5 time series points are 30-min averages

and 8 are examples of these time series plots, for U and e, which are of primary interest in this study. As before, the observations and the MM5 and WRF-NMM simulations are shown in each time series, and the HPAC-parameterised time series is shown only for e. Model values are all 30-min averages.

The U time series comparisons for 29 May in Fig. 7 suggest an RMSE difference of about $2\,\mathrm{m\,s^{-1}}$ (estimated by eye), with moderate mean biases of about 2 or $3\,\mathrm{m\,s^{-1}}$ persisting for several hours during a few periods. For example, the observed U averages about $2\,\mathrm{m\,s^{-1}}$ with a variability of about $\pm 1\,\mathrm{m\,s^{-1}}$ but with little trend from day to night. But MM5 predicts $4\,\mathrm{m\,s^{-1}}$ during the night and nearly calm during the day after about 1000 LST. WRF-NMM

tends to overpredict by an average of about 2 m s^{-1} all day. Of the 3 days analyzed, the best agreement can be seen on 7 June (not shown here), when all models follow the observed diurnal trends in U. On that day, WRF-NMM and MM5 have mean underprediction biases of about 1 and 2 m s^{-1}, respectively, during the daytime hours with MM5 speeds much closer to observed values during the nighttime hours.

Figure 8 shows the TKE time series at approximately 60 m for 6 June. Observed TKE is about 10–50 times greater during the afternoon than during the night. This magnitude of difference in e roughly agrees with the factor of six day-night difference in u_* that is found for these data, recognizing that e is proportional to the square of u_*. The two meteorological models are able to simulate this strong diurnal variation in TKE. However, the MM5 TKE prediction at night is often significantly less than the observed value and is close to the model's minimum value because of the very stable ABL regime being used in its closure scheme. The agreement between the meteorological models and the observations is better during the daytime, when there is a large increase beginning at sunrise, peaking at about 1200 to 1500 LST, and decreasing again towards sunset. The meteorological models are quite accurate in simulating the early morning increase, but tend to underpredict the afternoon TKE values by about 30–50%. The HPAC parameterised curve matches the observations fairly well, too, but has the same amount of underprediction in the afternoon.

Although we present no plots of the T time series, they suggest that the models simulate T values that are less, by about 4°C, than the observations for two of the three nights (29 May and 7 June). There is better agreement during the night of 6 June, except for WRF-NMM, which again has temperatures too low by about 2 or 3°C. The model T predictions during the day are closer (within about 1 or 2°C) to the observations, although the models have a fairly consistent 0.5–1.0°C underprediction bias. Note that these results are for a single location and are not necessarily representative of the entire simulated domains. For example, Reen (2007) reports that, for very similar MM5 simulations for these days, averaged over the 3 days and the entire domain, the nighttime T is about 0.9°C too high in the layer 0–150 m above the ground.

WD time series plots (not shown) suggest good agreement, within about ±20° much of the time. But for any given hour, the disagreement can be as much as 90°, with no indication of the reason. The smallest error in *WD* occurs on 7 June, which corresponds to the highest *WS*. This inverse dependence of *WD* uncertainty on U has been found in many other studies (e.g., Seaman 2000; Hanna and Yang 2001).

For u_*, the time series plots (not shown here) for the 3 days indicate a consistent diurnal variation in the observations, which average about 0.05 m s^{-1} at night and about 0.30 m s^{-1} in the day. However, there can be a factor of two or more observed variability from one 30-min period to the next. The HPAC parameterised values are generally about 0.3 m s^{-1} for the entire 24 h, thus indicating a factor of six overprediction at night, but minimal mean bias during the day. The nighttime overestimate is partly due to a mismatch between the assumed surface-layer profile shapes, since the stability corrections to the logarithmic wind law in MM5 do not match those in HPAC. But the main problem causing the discrepancy at night is the non-unique solution for u_* under very stable conditions given the inputs of U at a reference height and B_o. The latter problem is significant during very stable conditions, when the reference height, i.e., the lowest MM5 grid level with a U prediction, is not small in comparison with the MO length, L. Under these conditions, the HPAC surface-layer relations default to a near-neutral profile, generating a much larger value for u_* than the strongly stable MM5 value. The meteorological model-simulated u_* curves more correctly capture the day-night variation, although there is an average 50% to factor of two overprediction

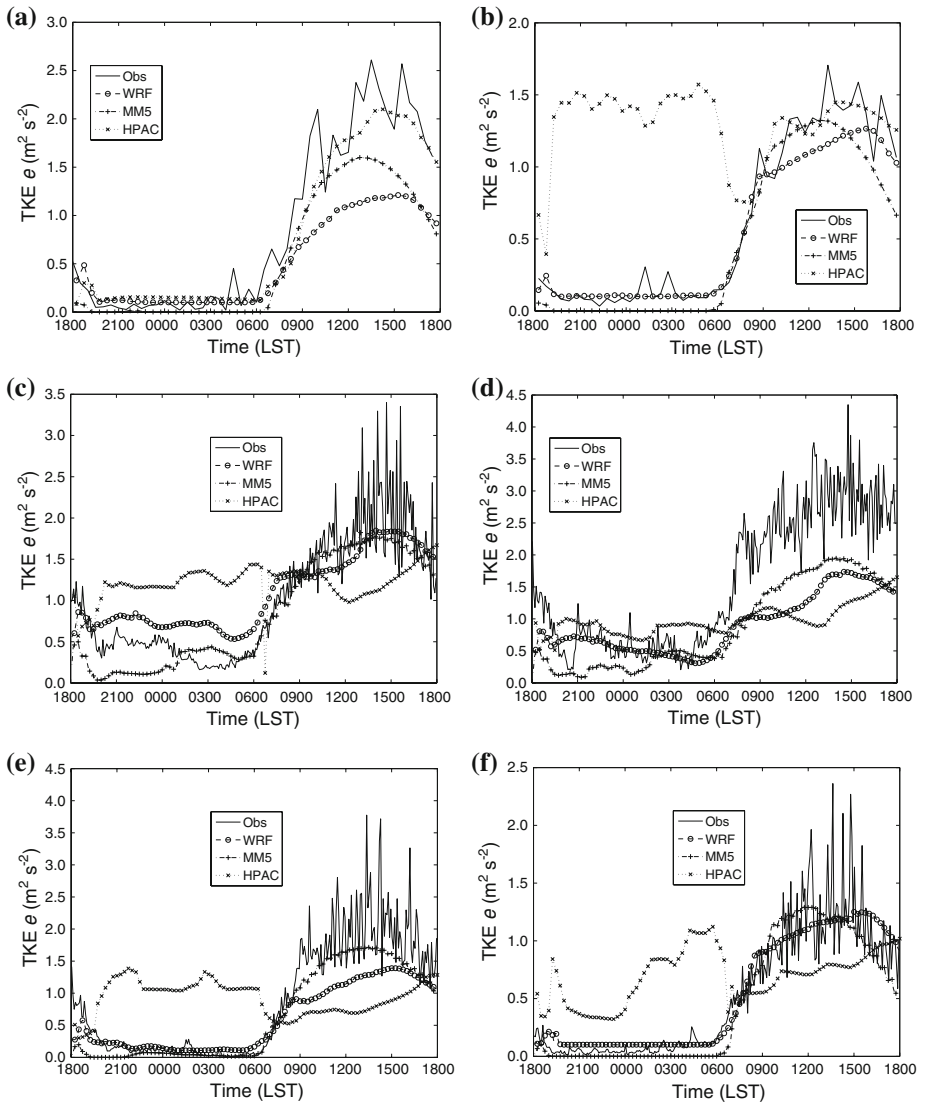

Fig. 9 **a** Observed ($z = 60$ m) and simulated (WRF 36 m, MM5 59 m, HPAC 60 m) e time series at CF1 for 1800 LST 6 June through 1800 LST 7 June. The WRF and MM5 time series points are 30-min averages. **b** Observed ($z = 2.1$ m) and simulated (WRF 36 m, MM5 59 m, HPAC 2.1 m) e time series at Smileyberg for 1800 LST 6 June through 1800 LST 7 June. The WRF and MM5 time series points are 30-min averages. **c** Observed ($z = 2.5$ m) and simulated (WRF 36 m, MM5 59 m, HPAC 2.5 m) e time series at ISFF1 for 1800 LST 6 June through 1800 LST 7 June. The WRF and MM5 time series points are 30-min averages. **d** Observed ($z = 2.7$ m) and simulated (WRF 36 m, MM5 59 m, HPAC 2.7 m) e time series at ISFF3 for 1800 LST 6 June through 1800 LST 7 June. The WRF and MM5 time series points are 30-min averages. **e** Observed ($z = 4.9$ m) and simulated (WRF 36 m, MM5 59 m, HPAC 4.9 m) e time series at ISFF6 for 1800 LST 6 June through 1800 LST 7 June. The WRF and MM5 time series points are 30-min averages. **f** Observed ($z = 4.7$ m) and simulated (WRF 36 m, MM5 59 m, HPAC 4.7 m) e time series at ISFF9 for 1800 LST 6 June through 1800 LST 7 June. The WRF and MM5 time series points are 30-min averages

bias most of the time. Also, the MM5-simulated u_* tends to have larger overpredictions (by 20–50% during the afternoon) than WRF-NMM.

The B_o time series for the nights of 29 May and 6 June (not shown) suggest that the observed and simulated values are all very close to zero. Most nighttime B_o elsewhere during clear skies have values of about -20 to $-50\,\mathrm{W\,m^{-2}}$, possibly because of clouds over the Lamont observing site, or possibly because that the sensible heat flux and latent heat flux cancel each other at this location on these two nights. On 7 June, the observed B_o remains near zero at night but the meteorological models estimate values of -10 to $-30\,\mathrm{W\,m^{-2}}$. The simulated daytime B_o match the observations quite well, on average. There is little mean bias during the daytime, although there may be a ± 100 to $300\,\mathrm{W\,m^{-2}}$ difference for any given 30-min average.

7.2 Comparisons of TKE Time Series for Six Sites for 7 June

The time series plots and discussions in Sect. 7.1 focused on the six major output variables of interest at the 60-m level of the Lamont, OK Central Facility, and included all three study days (29 May, 6 June and 7 June). The current section looks at only one output (TKE) and one day (7 June) but considers six of the 12 sites where TKE was observed. The TKE observations and meteorological model outputs are analyzed here because TKE is of most interest to the current study. There is one TKE time series plot in Fig. 9a through f for each of six representative sites out of the 12 available (Lamont Central Facility 1, Smileyberg, and ISFF 1, 3, 6, and 9, respectively). These sites are chosen randomly for presentation here. June 7 was chosen because it was marked by moderate winds from the south-east and no precipitation, otherwise it is a typical day.

During the day, simulations by the two meteorological models and the HPAC parameterisations are usually within a factor of two of the observed TKE for the six sites plotted in Fig. 9. MM5 and WRF-NMM estimates of e tend to be low by about 20% to a factor of two during the day, with MM5 nearly always predicting larger e than WRF-NMM.

During the night, the MM5 model is seen to simulate a very small background TKE for very stable conditions, which occur at about half of the sites. In Sect. 3.1, where the MM5 model is discussed, it is pointed out that the version being used does indeed default to a very small e near the surface during very stable conditions. The minimum background TKE is invoked for those times. But when MM5 does produce a value of e above its background value at night (see Fig. 9c, d), it is generally too low compared with the observations. The WRF-NMM model often simulates its minimum e ($0.1\,\mathrm{m^2\,s^{-2}}$), which may serendipitously agree with the observations. At other times at night, WRF-NMM simulates a larger e that is seen to agree fairly well with the observations with little overall bias. The HPAC-parameterised TKE has very large overestimates (up to a factor of 10–20) during the night at most of the sites. The three sites with better agreement between the HPAC parameterisations and the observations have moderately stable conditions and relatively high nighttime TKE. Because the nighttime ABL is less stable at these sites, the u_* estimate is more reliable. As mentioned earlier, the u_* estimate by HPAC is less reliable during very stable conditions, when the height of the U input is much larger than the MO length, L.

8 Conclusions and Suggestions for Further Studies

The IHOP ABL observations on three days have been compared with fields from versions of the MM5 and WRF-NMM meteorological models intended to be representative of opera-

tional versions and with the parameterisations of u_* and TKE by the HPAC dispersion model. The primary interest, though, is whether the meteorological models' turbulent kinetic energy (e) outputs are of sufficient accuracy to incorporate as inputs to HPAC. It is seen that, for these meteorological model applications with routine grid resolutions, the TKE simulations are adequate for the daytime, but that mean biases and scatter exist at night in very stable conditions.

In the radiosonde comparisons, well-defined observed mixing depths z_i are seen in only about half of the daytime soundings. For these soundings, the MM5 simulated z_i matches the observed values within about ±20 to 40% and have little mean bias. The WRF-NMM mixing depths have similar scatter but are too high by about 30% on average. At night, the observed z_i are often too shallow (e.g., 20 m or less) to be resolved by the radiosondes or the meteorological models, due to their relatively coarse resolution. When compared with the U profiles observed by the radiosondes, the meteorological model simulated U profiles in the ABL often have biases of 2–4 m s^{-1}, which are thought to be generally due to slight misplacement of fronts or waves in time and space. After the mean bias is removed, the scatter is still about 1 or 2 m s^{-1}, similar to that found in previous comparisons.

The time series plots were compared for several ABL variables near the surface at Lamont, Oklahoma. Coarse vertical resolution contributes to the meteorological models usually (but not always) underpredicting the nighttime T by several °C. Agreement is better during the daytime. As expected, there is scatter between the meteorological model and the observed nighttime WD, while the daytime WD has fair agreement (±20°) most of the time. Agreement is better on the day (7 June) with steady moderate winds. The simulated U has an RMSE of about 2 m s^{-1} and sometimes large mean biases, and the meteorological models' u_* simulations tend to follow the large (factor of 10) diurnal variation of the observations with typical scatter of less than a factor of two. The HPAC parameterisation of u_* is much too large at night, due primarily to the fact that the lowest meteorological model height for wind calculation is too high for the HPAC solution method. The height of the U input should be less than about $5L$ for the u_* solution to converge. The meteorological models' TKE simulations (available only at the top of the lowest grid volume, or approximately 35 m for WRF and 59 m for MM5) are fairly good (within about a factor of two) during the daytime, but tend to underpredict the mid-afternoon maximum by about 30–40%. The HPAC parameterised TKE has a slight underprediction trend during the day. At night, when u_* is overpredicted by HPAC, e is also greatly overpredicted (by a factor of two to five). B_o is observed to be close to zero at night and the meteorological models agree, while during the day, the models match the general cosine curve of B_o, although the scatter is about ±20 to 40%.

Focusing on TKE and considering all 12 sonic anemometer sites, it is found that, during the daytime, the meteorological model simulations and the HPAC parameterisations of TKE are usually within a factor of two of the observations. On average, the MM5 and WRF-NMM simulations are low by about 20–50%. The HPAC TKE value is about 30% to a factor of two less than the observed value. During the nighttime, the observed TKE value is much smaller than during the day, and the WRF-NMM model simulations are within a factor of two much of the time with its assumed minimum of 0.1 m^2 s^{-2}. The MM5 TKE outputs are often close to zero at night because of its ABL closure scheme and assumed minimum of 0.001 m^2 s^{-2}. The HPAC parameterised TKE is usually much too large, by a factor of 10–20, attributed to its overestimate of u_*.

Based on these results, the following primary conclusions/recommendations are:

(1) We recognize the fact that meteorological models have traditionally focused on accurate simulations of weather phenomena that are of most interest to the public (e.g.,

high winds, high or low temperatures, rain and snow), and that are of most use in climate assessments (e.g., surface energy balance components). There has been less effort devoted to ABL parameters of interest to dispersion modelling, such as z_i, e and profiles of U in the surface layer. Turbulent kinetic energy and other ABL variables are least well-simulated on very stable nights, when the meteorological models default to their assumed minimum or background e, which differs by a factor of 100 between MM5 GS and WRF-NMM MYJ.

(2) The lowest meteorological model grid volume has a thickness of approximately 35 m (for WRF-NMM) and 59 m (for MM5) in this study. The e is computed at the interfaces of model layers and so these heights are the lowest at which e is simulated directly by the model. However, U is calculated at the centres of these layers and so the lowest heights at which U is simulated directly by the models are approximately 18 m (WRF-NMM) and 30 m (MM5). Dispersion models, such as HPAC, need these variables at lower heights. The formulation of the stability correction in the logarithmic wind law varies among MM5 GS, WRF-NMM MYJ and HPAC. It would be better to use consistent MO similarity relations in the meteorological models and in HPAC. For HPAC, this involves an iterative approach as described below.

(3) As seen in the HPAC evaluations here, its methods of estimating u_* (and hence e) and the U and T profiles in the lowest grid volume are based on input of the meteorological model simulated U at the middle of the lowest model grid volume, z_o, and B_o. As with other operational dispersion models, HPAC then iterates between u_* and L until the solution converges. But if the height of the middle of the lowest model grid volume is $> 5L$, the U input is at a height above the implied surface layer and the solution is indeterminate and has trouble converging. In our study, this led to large overestimates of u_* and e by HPAC during stable nights.

(4) One solution to the previous two issues is to increase the vertical resolution (i.e., decrease the depth of the lowest grid volume) in the meteorological models near the ground. For example, a lowest grid depth of 10 m would be an improvement. Recent modelling with the advanced research version of WRF using MYJ with 2-m grid spacing near the surface and 10 layers below 50 m has shown promise in stable conditions (e.g., Stauffer et al. 2009).

(5) Until the above issues are resolved, the use of a meteorological model for the evaluation of TKE in dispersion models at heights less than about 50 m is not recommended for nighttime stable periods. Similarly, the use of a meteorological model U in the middle of the coarse resolution lowest grid volumes to estimate u_* and e is not recommended in stable conditions.

Acknowledgements This research has been sponsored by the Defense Threat Reduction Agency, with CDR Stephanie Hamilton and Dr. John Hannan as the program managers. The authors appreciate the assistance provided by Ric Cederwall and Mark Fischer of LLNL and David Cook of ANL in acquiring the IHOP turbulence data and carrying out additional processing. The authors also thank Fei Chen and Kevin Manning for providing offline Noah output for initialization of MM5 LSM fields.

References

Ballard SP, Golding BW, Smith RNB (1991) Mesoscale model experimental forecasts of the Haar of northeast Scotland. Mon Weather Rev 119:2107–2123

Benjamin KJ, Seaman NL (1985) A simple scheme for objective analyses in curved flow. Mon Weather Rev 113:1184–1198

Blackadar AK (1962) The vertical distribution of wind and turbulent exchange in a neutral atmosphere. J Geophys Res 67:3095–3102
Chen F, Dudhia J (2001) Coupling an advanced land surface-hydrology model with the Penn State-NCAR MM5 modeling system. Part I: Model implementation and sensitivity. Mon Weather Rev 129:569–585
Chen F, Manning KW, LeMone MA, Trier SB, Alfieri JG, Roberts R, Tewari M, Niyogi D, Horst TW, Onley SP, Basara JB, Blanken PD (2007) Description and evaluation of the characteristics of the NCAR high-resolution land data assimilation system. J Appl Meteorol Clim 46:694–713
Cox R, Bauer BL, Smith T (1998) A mesoscale model intercomparison. Bull Amer Meteorol Soc 79:265–283
Deng A, Stauffer DR (2006) On improving 4-km mesoscale model simulations. J Appl Meteorol Clim 43:1864–1886
DTRA (2004) HPAC version 4.04.011 (DVD containing model and accompanying data and document files). DTRA, Ft. Belvoir, VA
Dudhia J (1993) A nonhydrostatic version of the Penn State/NCAR mesoscale model: validation tests and simulation of an Atlantic cyclone and cold front. Mon Weather Rev 121:1493–1513
Grell GA, Dudhia J, Stauffer DR (1995) A description of the fifth-generation Penn State/NCAR Mesoscale Model (MM5). NCAR/TN-398+STR. National Center for Atmospheric Research, Boulder, CO, 122 pp
Hanna SR, Yang R (2001) Evaluations of mesoscale model predictions of near-surface winds, temperature gradients, and mixing depths. J Appl Meteorol 40:1095–1104
Janjic ZI (1996a) The Mellor-Yamada level 2.5 scheme in the NCEP Eta model. In: 11th conference on NWP, Norfolk, VA, 19–23 Aug 1996. American Meteorological Society, Boston, pp 333–334
Janjic ZI (1996b) The surface layer in the NCEP Eta model. In: 11th conference on NWP, Norfolk, VA. American Meteorological Society, Boston, pp 354–355
Janjic ZI (2001) Nonsingular implementation of the Mellor-Yamada Level 2.5 scheme in the NCEP Meso model. NCEP Office note no. 437, pp 61
Janjic ZI (2003) A nonhydrostatic model based on a new approach. Meteorol Atmos Phys 82:271–285. Online: http://dx.doi.org/10.1007/s00703-001-0587-6
Kain JS, Fritsch JM (1990) A one-dimensional entraining/detraining plume model. J Atmos Sci 47:2784–2802
Kang SL (2007) The effects of mesoscale surface heterogeneity on the fair-weather convective atmospheric boundary layer. Ph.D. Dissertation, Pennsylvania State University, 200 pp. Available from the Department of Meteorology, The Pennsylvania State University, University Park, PA
Kang SL, Davis KJ, LeMone MA (2007) Observations of ABL structures over a heterogeneous land surface during IHOP-2002. J Hydrometeorol 8:221–244
LeMone MA, Chen F, Alfieri JG, Cuenca RH, Hagimoto Y, Blanken P, Niyogi D, Kang S, Davis K, Grossman RL (2007a) NCAR/CU surface, soil, and vegetation observations during the International H_2O Project 2002 field campaign. Bull Amer Meteorol Soc 88:65–81
LeMone MA, Chen F, Alfieri JG, Tewari M, Geerts B, Miao Q, Grossman RL, Coulter RL (2007b) Influence of land cover and soil moisture on the horizontal distribution of sensible and latent heat fluxes in Southeast Kansas during IHOP-2002 and CASES-97. J Hydrometeorol 8:68–87
Mlawer EJ, Taubman SJ, Brown PD, Iacono MJ, Clough SA (1997) Radiative transfer for inhomogeneous atmosphere: RRTM, a validated correlated-K model for the longwave. J Geophys Res 102(D14):16663–16682
Pielke RASr (1998) The need to assess uncertainty in air quality evaluations. Atmos Environ 32:1467–1468
Pielke RASr, Uliasz M (1998) Use of meteorological models as input to regional and mesoscale air quality models—limitations and strengths. Atmos Environ 32:1455–1466
Reen BP (2007) Data assimilation strategies and land-surface heterogeneity effects in the planetary boundary layer. Ph.D. Dissertation. Pennsylvania State University, 246 pp. Available from the Department of Meteorology, The Pennsylvania State University, University Park, PA, http://etda.libraries.psu.edu/
Seaman NL (2000) Meteorological modeling for air quality assessments. Atmos Environ 34:2231–2259
Seaman NL, Stauffer DR, Lario-Gibbs AL (1995) A multi-scale four-dimensional data assimilation system applied to the San Jouquin Valley during SARMAP. Part I: Modeling design and basic performance characteristics. J Appl Meteorol 34:1739–1761
Shafran PC, Seaman NL, Gayno GA (2000) Evaluation of numerical predictions of boundary layer structure during the Lake Michigan Ozone Study. J Appl Meteorol 39:412–426
Skamarock WC (2004) Evaluating mesoscale NWP models using kinetic energy spectra. Mon Weather Rev 132:3019–3032
Stauffer DR, Seaman NL (1994) Multiscale four-dimensional data assimilation. J Appl Meteorol 33:416–434
Stauffer DR, Muñoz RC, Seaman NL (1999) In-cloud turbulence and explicit microphysics in the MM5. In: 9th PSU/NCAR MM5 modeling system users' workshop, NCAR, Boulder, CO, pp 177–180

Stauffer DR, Seaman NL, Hunter GK, Leidner SM, Lario-Gibbs AM, Tanrikulu S (2000) A field-coherence technique for meteorological field-program design for air-quality studies. Part I: Description and interpretation. J Appl Meteorol 39:297–316

Stauffer DR, Muñoz RC, Seaman NL (2001) On the importance of saturation effects in the turbulence scheme of a mesoscale model. In: 9th AMS conference on mesoscale processes, Ft. Lauderdale, FL, 30 July–2 August, pp 1–5

Stauffer DR, Hunter GK, Deng A, Zielonka JR, Tinklepaugh K, Hayes P, Kiley C (2007) On the role of atmospheric data assimilation and model resolution on model forecast accuracy for the Torino Winter Olympics. In: 22nd conference on weather analysis and forecasting/18th conference on NWP, Park City, Utah. American Meteorological Society. Extended abstract 11A.6, available at http://ams.confex.com/ams/22WAF18NWP/techprogram/paper_124791.htm

Stauffer DR, Gaudet BJ, Seaman NL, Wyngaard JC, Mahrt L, Richardson S (2009) Sub-kilometer numerical predictions in the nocturnal stable boundary layer. In: 23rd American Meteorological Society conference on weather analysis and forecasting/19th American Meteorological Society conference on numerical weather prediction, Omaha, Nebraska, USA, 1–5 June, 18B.4

Sykes RI, Parker S, Henn D, Chowdhury B (2007) SCIPUFF version 2.3 technical documentation. L-3 Titan Corp, Princeton, NJ, 336 pp

Tanrikulu S, Stauffer DR, Seaman NL, Ranzieri AJ (2000) A field-coherence technique for meteorological field-program design for air-quality studies. Part II: Evaluation in the San Joaquin Valley. J Appl Meteorol 39:317–334

Weckwerth TM, Parsons DB, Koch SE, Moore JA, LeMone MA, Demoz BB, Flamant C, Geerts B, Wang J, Feltz WF (2004) An overview of the International H2O Project (IHOP-2002) and some preliminary highlights. Bull Amer Meteorol Soc 85:253–277

Yamada T (1977) A numerical experiment on pollutant dispersion in a horizontally homogenous atmospheric boundary layer. Atmos Environ 11:1015–1024

Zhang D, Anthes RA (1982) A high-resolution model of the Planetary Boundary Layer—sensitivity tests and comparisons with SESAME-79 data. J Appl Meteorol 21:1594–1607